AJNR

Diagnostic Performance of Dynamic Contrast-Enhanced 3T MR Imaging for Characterization of Orbital Lesions: Validation in a Large Prospective Study

Emma O'Shaughnessy, Chloé Le Cossec, Natasha Mambour, Adrien Lecoeuvre, Julien Savatovsky, Mathieu Zmuda, Loïc Duron and Augustin Lecler

AJNR Am J Neuroradiol 2024, 45 (3) 342-350
doi: https://doi.org/10.3174/ajnr.A8131
http://www.ajnr.org/content/45/3/342

Diagnostic Performance of Dynamic Contrast-Enhanced 3T MR Imaging for Characterization of Orbital Lesions: Validation in a Large Prospective Study

Emma O'Shaughnessy, Chloé Le Cossec, Natasha Mambour, Adrien Lecoeuvre, Julien Savatovsky, Mathieu Zmuda, Loïc Duron, and Augustin Lecler

ABSTRACT

BACKGROUND AND PURPOSE: Orbital lesions are rare but serious. Their characterization remains challenging. Diagnosis is based on biopsy or surgery, which implies functional risks. It is necessary to develop noninvasive diagnostic tools. The goal of this study was to evaluate the diagnostic performance of dynamic contrast-enhanced MR imaging at 3T when distinguishing malignant from benign orbital tumors on a large prospective cohort.

MATERIALS AND METHODS: This institutional review board–approved prospective single-center study enrolled participants presenting with an orbital lesion undergoing a 3T MR imaging before surgery from December 2015 to May 2021. Morphologic, diffusion-weighted, and dynamic contrast-enhanced MR images were assessed by 2 readers blinded to all data. Univariable and multivariable analyses were performed. To assess diagnostic performance, we used the following metrics: area under the curve, sensitivity, and specificity. Histologic analysis, obtained through biopsy or surgery, served as the criterion standard for determining the benign or malignant status of the tumor.

RESULTS: One hundred thirty-one subjects (66/131 [50%] women and 65/131 [50%] men; mean age, 52 [SD, 17.1] years; range, 19–88 years) were enrolled. Ninety of 131 (69%) had a benign lesion, and 41/131 (31%) had a malignant lesion. Univariable analysis showed a higher median of transfer constant from blood plasma to the interstitial environment (K^{trans}) and of transfer constant from the interstitial environment to the blood plasma (minute^{-1}) (Kep) and a higher interquartile range of K^{trans} in malignant-versus-benign lesions (1.1 minute^{-1} versus 0.65 minute^{-1}, $P = .03$; 2.1 minute^{-1} versus 1.1 minute^{-1}, $P = .01$; 0.81 minute^{-1} versus 0.65 minute^{-1}, $P = .009$, respectively). The best-performing multivariable model in distinguishing malignant-versus-benign lesions included parameters from dynamic contrast-enhanced imaging, ADC, and morphology and reached an area under the curve of 0.81 (95% CI, 0.67–0.96), a sensitivity of 0.82 (95% CI, 0.55–1), and a specificity of 0.81 (95% CI, 0.65–0.96).

CONCLUSIONS: Dynamic contrast-enhanced MR imaging at 3T appears valuable when characterizing orbital lesions and provides complementary information to morphologic imaging and DWI.

ABBREVIATIONS: AUC = area under the curve; DCE = dynamic contrast-enhanced; ICC = intraclass correlation coefficient; IQR = interquartile range; Kep = constant of transfer from the interstitial environment to the blood plasma (minute^{-1}); K^{trans} = Constant of transfer from blood plasma to the interstitial environment (minute^{-1}); OCVM = orbital cavernous venous malformation; ROC = receiver operating characteristic; TIC = time-intensity curve; Ve = extravascular-extracellular volume per unit of volume of tissue (mL/100mL of tissue; %); Vp = plasmatic volume per unit of volume of tissue (mL/100mL of tissue; %); WI = weighted imaging

Orbital lesions constitute a heterogeneous group, with various histopathologies, which are difficult to characterize solely by clinical examination and imaging. Among the most common benign orbital lesions, vascular malformations are prominent, with cavernous orbital malformation being by far the most frequent benign tumor in adults. Additionally, there is a group of orbital inflammations that encompasses both idiopathic and specific inflammations, involving a wide range of causes. Among the most common malignant orbital lesions, lymphoma is the most frequent tumor, especially in the elderly. Carcinomas are also relatively common lesions. A particular diagnostic challenge lies in distinguishing orbital inflammation from lymphomas because they often exhibit similar morphologic features on imaging.[1,2] Histologic evidence obtained by biopsy or surgery remains the milestone for characterizing orbital lesions. However, biopsy or complete removal of an orbital lesion might be challenging and even dangerous. Indeed, all orbital surgery is complex due to the numerous vascular, nervous, and muscular structures within the orbit, which entail a non-negligible risk to both aesthetic and functional outcomes.[3,4]

Received October 6, 2023; accepted after revision December 5.

From the Departments of Neuroradiology (E.O., J.S., L.D., A.L.), Clinical Research (C.L.C., A.L.), and Ophthalmology (N.M., M.Z.), Rothschild Foundation Hospital, Paris, France.

Please address correspondence to Emma O'Shaughnessy, MD, MPH, Department of Neuroradiology, Rothschild Foundation Hospital, 25 rue Manin, 75019 Paris, France; e-mail: eoshaughnessy@for.paris

Indicates article with online supplemental data.

http://dx.doi.org/10.3174/ajnr.A8131

Developing noninvasive techniques for characterization, such as imaging, is therefore crucial and valuable to avoid unnecessary surgery in patients with benign lesions. A few imaging techniques proved useful to characterize orbital lesions. Color Doppler ultrasound measures the resistance index in lesion vessels. MR imaging gives specific imaging findings such as an enlarged infraorbital nerve, the apparent diffusion coefficient (ADC), or the intravoxel incoherent motion.[5-13]

Dynamic contrast-enhanced (DCE) imaging is another advanced MR imaging technique, allowing direct quantification of the perfusion volumes as well as an estimation of the capillary permeability, reflecting the tumor microcirculation.[14] It is, therefore, a valuable technique for the characterization of orbital lesions. DCE showed valuable results for assessing aggressiveness in optic pathway gliomas, lymphoproliferative disorders, and lacrimal gland tumors.[15-17] However, only a few studies have evaluated this technique in the orbit so far. Most evaluated small series of patients or were retrospective. Various approaches have been documented in the literature, encompassing qualitative, semiquantitative, or quantitative methods to evaluate DCE, along with the use of complex pharmacodynamic models. Consequently, a range of metrics has been suggested. Among these, the most promising ones for characterizing orbital lesions were the area under the curve AUC_{DCE} (millimol.liter^{-1}.minute), the constant of transfer from the interstitial environment to the blood plasma (minute^{-1}) (Kep), and the constant of transfer from blood plasma to the interstitial environment (minute^{-1}) (K^{trans}).[15,16,18-26] K^{trans} represents the rate constant for the transfer of substances from the blood plasma to the interstitial environment, while Kep (minute^{-1}) signifies the rate constant for the reverse transfer from the interstitial environment back to the blood plasma. By means of the extended Tofts pharmacokinetic model, one can obtain 2 other parameters: Ve (milliliter/100mL of tissue; %) (the extravascular-extracellular volume within a given volume of tissue) and Vp; the plasmatic volume within the same unit of tissue volume.

The goal of this study was to evaluate the diagnostic performance of DCE MR imaging at 3T when distinguishing malignant from benign orbital tumors on a large prospective cohort. This work is involved in the validation process of a new diagnostic imaging tool and biomarkers. It contributes to improving the level of evidence on the value of DCE MR for the diagnostic management of orbital tumors.

MATERIALS AND METHODS

Research Design

A prospective single-center study was conducted in a tertiary center specializing in ophthalmic diseases (NCT02434120). This study was approved by an Institutional Research Ethics Board and adhered to the tenets of the Declaration of Helsinki. Our study follows the Standards for Reporting of Diagnostic Accuracy Studies guidelines. Signed informed consent was obtained from all subjects.

Population

A total of 345 participants were enrolled from December 2015 to May 2021.

Inclusion criteria were the following: 1) older than 18 years of age, 2) the presence of an orbital mass for which a biopsy or a complete removal was planned, and 3) MR imaging completed before surgery.

Primary exclusion criteria were the following: 1) absolute or relative contraindication to MR imaging or to an injection of gadolinium, 2) opposition of the patient to participating in the study, and 3) absence of an affiliation to the social welfare system.

Secondary exclusion criteria were the following: 1) artifacts preventing analysis of the area of interest, 2) biopsy or surgery not performed, and 3) MR image analysis allowing a diagnosis considered as certain.

For all patients, no treatment that may alter imaging, such as steroids, and no surgery or biopsy was undertaken before MR imaging.

The final study cohort enrolled 131 participants. A flow chart is given in Fig 1.

Clinical and Ophthalmologic Data

The clinical examination and management of patients was performed by a team of ophthalmologists specialized in orbital surgery at our institution. Medical history (cancer, autoimmune disease, HIV seropositivity, diabetes, hypertension, smoking) and clinical symptoms (diplopia, vision loss, exophthalmos, palpebral inflammation, ptosis) were noted. Fundoscopy was performed to detect optic disc edema and optic nerve atrophy. Oculomotricity testing was performed.

Reference Standard

Histopathology was assessed, by an experienced pathologist, blinded to imaging data, who specialized in orbital pathology with 30 years of experience and was considered the reference standard. Orbital lesions were classified as malignant or benign. For further analysis, subgroups of lymphomas and orbital inflammations were extracted from malignant and benign lesions, respectively.

MR Imaging Protocol

All orbital MR images were obtained on the same 3T Ingenia system (Philips Healthcare). The MR imaging protocol is shown in the Online Supplemental Data. DCE MR imaging acquisitions were based on a 3D T1 fast-field echo sequence with a temporal resolution of 2.9 seconds and a total duration of 6 minutes 23 seconds after an injection of a 0.1-mmol/kg bolus of gadobutrol (Gadovist; Bayer) at a speed of 4 mL/s. Participants were asked to look at a fixed point during the acquisitions to prevent kinetic artifacts generated by eye movement.

Imaging Analysis

The morphologic analysis was performed by a senior neuroradiologist (A.L.) with >10 years of experience in orbital imaging, blinded to all data.

The reader assessed the following characteristics of each orbital lesion:

- Center of the lesion: lacrymal gland, orbital fat, eyelid, muscle, bone
- Boundaries, defined as regular or irregular
- Shape, defined as regular or irregular
- Type, defined as infiltrative with ill-defined margins or well-delineated with sharply defined margins

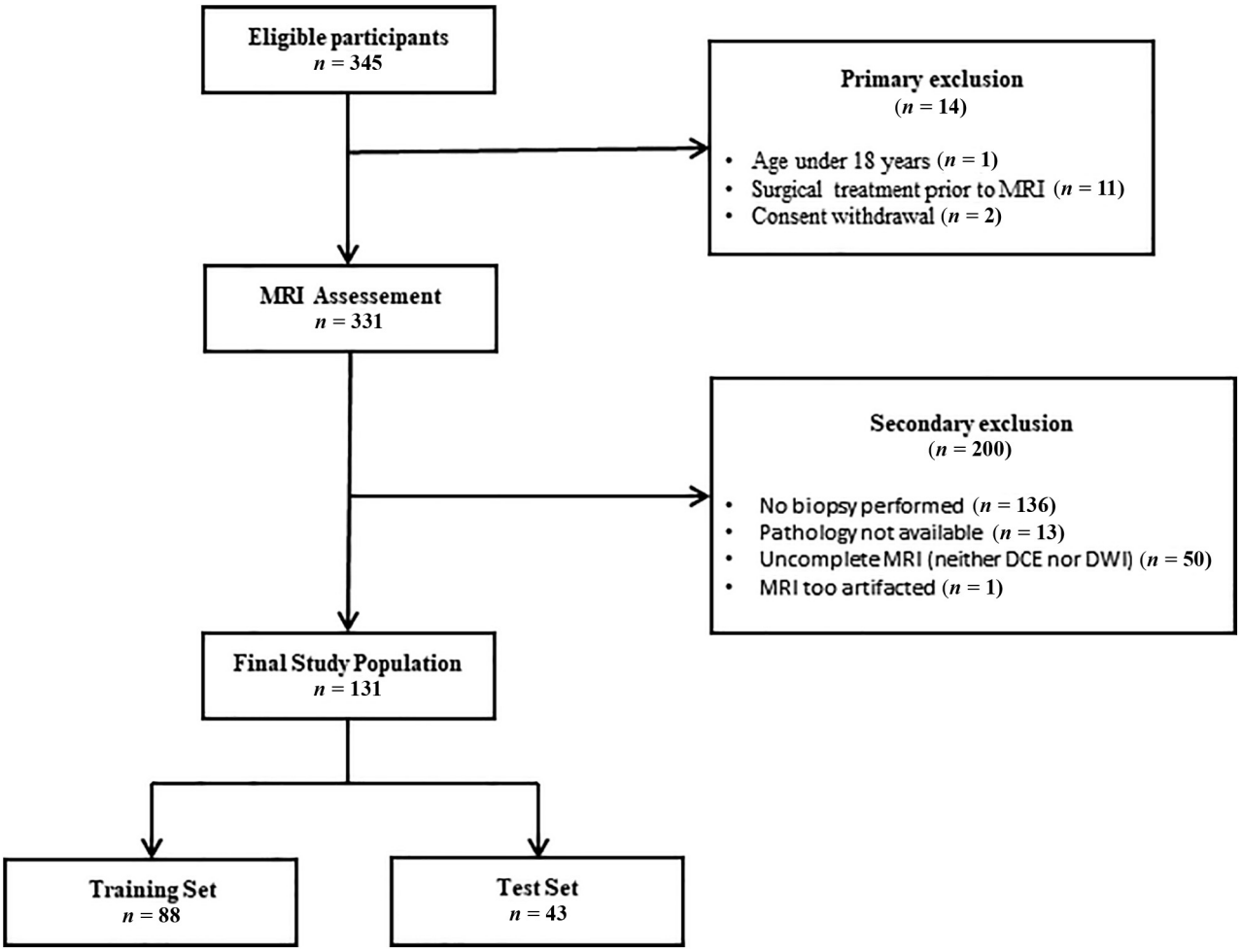

FIG 1. Flow chart.

- Signal intensity on T1WI and T2WI, defined as hypointense, isointense, or hyperintense in comparison with the signal intensity of a healthy ipsilateral or contralateral extraocular muscle (defined by normal morphology and signal)
- Signal intensity on DWI defined as hypointense, isointense, or hyperintense in comparison with the signal intensity of a healthy ipsilateral or contralateral extraocular muscle
- Signal intensity on the ADC map, defined as hypointense, isointense, or hyperintense in comparison with the signal intensity of a healthy ipsilateral or contralateral extraocular muscle
- Type of enhancement, defined as homogeneous or heterogeneous
- Enhancement intensity on contrast-enhanced T1WI, defined as absent, lower than that of the extraocular muscle, equal to that of the extraocular muscle, or higher than that of the extraocular muscle.

DCE MR Imaging Postprocessing and Analysis

All the postprocessing steps were performed using Olea Sphere software (Version 3.0; Olea Medical). Postprocessing was performed by a radiologist in training with 3 years of experience (E.O.). It lasted <1 minute. A 2D single-section ROI, encompassing the maximum area of the lesion, was manually drawn on each lesion on the AUC_{DCE} colored map by the same radiologist in training, as recommended by Qian et al.[27] A second ROI was manually drawn on the same lesion and at the same level on the ADC colored map. A second reading was done by the senior neuroradiologist (L.D.) to evaluate the interreader reproducibility.

A qualitative assessment of the DCE time-intensity curve (TIC) was made, classified into 3 types, according to Yuan et al:[18] type 1, defined as the persistent pattern with straight or curved lines and continuous enhancement over the entire dynamic study; type 2, defined as the plateau pattern with a relatively prominent increase of slope and a final intensity of 90%–100% of the peak grade; and type 3, defined as the washout pattern with a rapid increase of slope and a final intensity lower than 90% of the peak grade.

The AUC_{DCE} (millimol.liter^{-1}.minute), which is a semiquantitative parameter reflecting the relative quantity of contrast agent with time, was obtained by a model-free analysis of the TIC.

An extended Tofts pharmacokinetic model was then used, on the basis of Bayesian probabilities performing a biexponential modeling of diffusion, providing the 4 following quantitative parameters: K^{trans}, Kep, Ve, and Vp.[28]

Both the median and interquartile range (IQR) were obtained for each DCE parameter. The median, which is a positional parameter less affected by extreme values than the mean, and the IQR, which gives information about the statistical dispersion,

Table 1: Participant characteristics and lesion histopathologies

Mean (SD) or No. (%)	Whole Sample ($n = 131$)
Age	52 (17.1) (range, 19–88)
Sex	
Female	66/131 (50.4%)
Male	65/131 (49.6%)
Histopathology	
Benign lesion	
Overall	90/131 (68.7%)
Orbital inflammation	43/131 (32.8%)
Orbital cavernous venous malformation	9/131 (6.9%)
Other benign lesion	38/131 (29.0%)
Malignant lesion	
Overall	41/131 (31.3%)
Lymphoma	20/131 (15.3%)
Primary solid malignant tumor	12/131 (6.9%)
Solid tumor metastasis	9/131 (9.2%)
Bilateral lesion	22/131 (16.8%)

provide distinct information and thus are not considered redundant. Colored maps were displayed for all parameters.

Statistical Methods

For all quantitative variables, the mean and standard deviation (SD) were provided. For all qualitative variables, both the number and percentage were given.

A univariable analysis was performed. For quantitative variables, a *t* test with a Welch correction if necessary or a Wilcoxon test was used. For qualitative variables, χ^2 or Fisher tests were used. Given the exploratory approach of this step, we did not correct for the α inflation risk. The analysis was conducted for 2 comparisons: malignant-versus-benign lesions and lymphoma-versus-orbital inflammation.

A multivariable analysis was then performed using logistic regressions. The whole data set of patients was divided randomly into a training and a test set, with a respective proportion of two-thirds and one-third. We considered 4 models: model A with DCE parameters; model B with DCE parameters and ADC; model C with DCE and morphologic imaging parameters; and model D with DCE, ADC, and morphologic imaging parameters. Three additional models were also considered without DCE: model E with morphologic imaging parameters alone, model F with ADC alone, and model G with morphologic imaging parameters and ADC.

For each model, variables with a *P* value < 20% in univariable analysis were considered. A stepwise procedure based on the Akaike criterion was used to select the relevant parameters.

For each parameter of DCE and each model, a receiver operating characteristic (ROC) curve with a 95% confidence interval was drawn, and the AUC was computed. Sensitivity and specificity were calculated when AUCs were >0.80. The Youden method was used for threshold identification. Confidence intervals for the model ROC curves and AUC were obtained by a bootstrap technique. The *P* value for the AUC was obtained using the DeLong test, at 5% α risk.

The interobserver agreement was evaluated using the Bland-Altman limits of agreement and an intraclass correlation coefficient (ICC) with 95% confidence intervals for quantitative variables[29] and the Cohen κ for qualitative variables.

Analyses were performed using the R statistical and computing software, Version 4.2.0 (http://www.r-project.org/) by a methodologist statistician (C.L.C) with 8 years of experience.

RESULTS

Study Population

A total of 131 patients, 66/131 [50%] women and 65/131 [50%] men (mean age, 52 [SD, 17.1] years; range, 19–88 years) were enrolled, among whom 41/131 (31%) had malignant lesions. Participant characteristics and lesion histopathologies are available in Table 1. More details on histopathologies can be found in the Online Supplemental Data.

Distinction between Malignant and Benign Orbital Lesions

Univariable Analysis. Patients with a malignant lesion were significantly older than those with a benign one: 62.4 (SD, 15.4) versus 47.3 (SD, 15.8) years, $P < .001$.

Regarding the morphologic features, there was a significant difference in DWI and ADC signal, enhancement intensity, and the type of TIC between patients with a malignant lesion compared with those with a benign lesion ($P < .001$).

Among all DCE parameters, the medians of K^{trans} and Kep and the IQR of K^{trans} were significantly higher in malignant lesions compared with benign lesions: 1.1 $minute^{-1}$ versus 0.65 $minute^{-1}$, $P = .03$; 2.1 $minute^{-1}$versus 1.1 $minute^{-1}$, $P = .01$; and 0.81 $minute^{-1}$ versus 0.37 $minute^{-1}$, $P = .009$, respectively. The median of the AUC_{DCE} was significantly lower in malignant lesions compared with benign ones: 3.8×10^4 versus 5.4×10^4, $P = .01$. The median of the ADC was significantly lower in malignant lesions compared with benign ones: 0.86 versus 1.2 mm^2/s, $P = .001$. The detailed data for both groups are given in the Online Supplemental Data.

ROC Curves for Each DCE Parameter and ADC. The parameters with the highest AUC were the median of Kep, the IQR of Kep, and the IQR of K^{trans} with AUCs of 0.74 (95% CI, 0.65-0.83), 0.73 (95% CI, 0.64–0.82), and 0.71 (95% CI, 0.61–0.80), respectively. The AUC of the median and the IQR of the ADC were, respectively, 0.74 (95% CI, 0.63–0.85) and 0.6 (95% CI, 0.48–0.72). The ROC curves of each DCE parameter and ADC are shown in Fig 2.

Multivariable Analysis. The training set included 88 patients, and the test set, 43 patients, with 26 and 15 malignant lesions, respectively. The model with the highest diagnostic performance was model D (DCE, ADC, and morphologic imaging features), with an AUC = 0.81 (95% CI, 0.67–0.96) (*P* value = 1.6×10^{-5}, in comparison with an AUC of 0.5), sensitivity = 0.82 (95% CI, 0.55–1), and specificity = 0.81 (95% CI, 0.65–0.96). The Online Supplemental Data show the diagnostic performance of models evaluated, and ROC curves are available in Fig 3.

Model D had a sensitivity of 0.82 (95% CI, 0.55–1) and a specificity of 0.81 (95% CI, 0.65–0.96), with 2 false-negatives and 5 false-positives. Model E had a specificity of 0.48 (95% CI, 0.3–0.67) with 14 false-positives. Model F showed a sensitivity of 0.5 (95% CI,

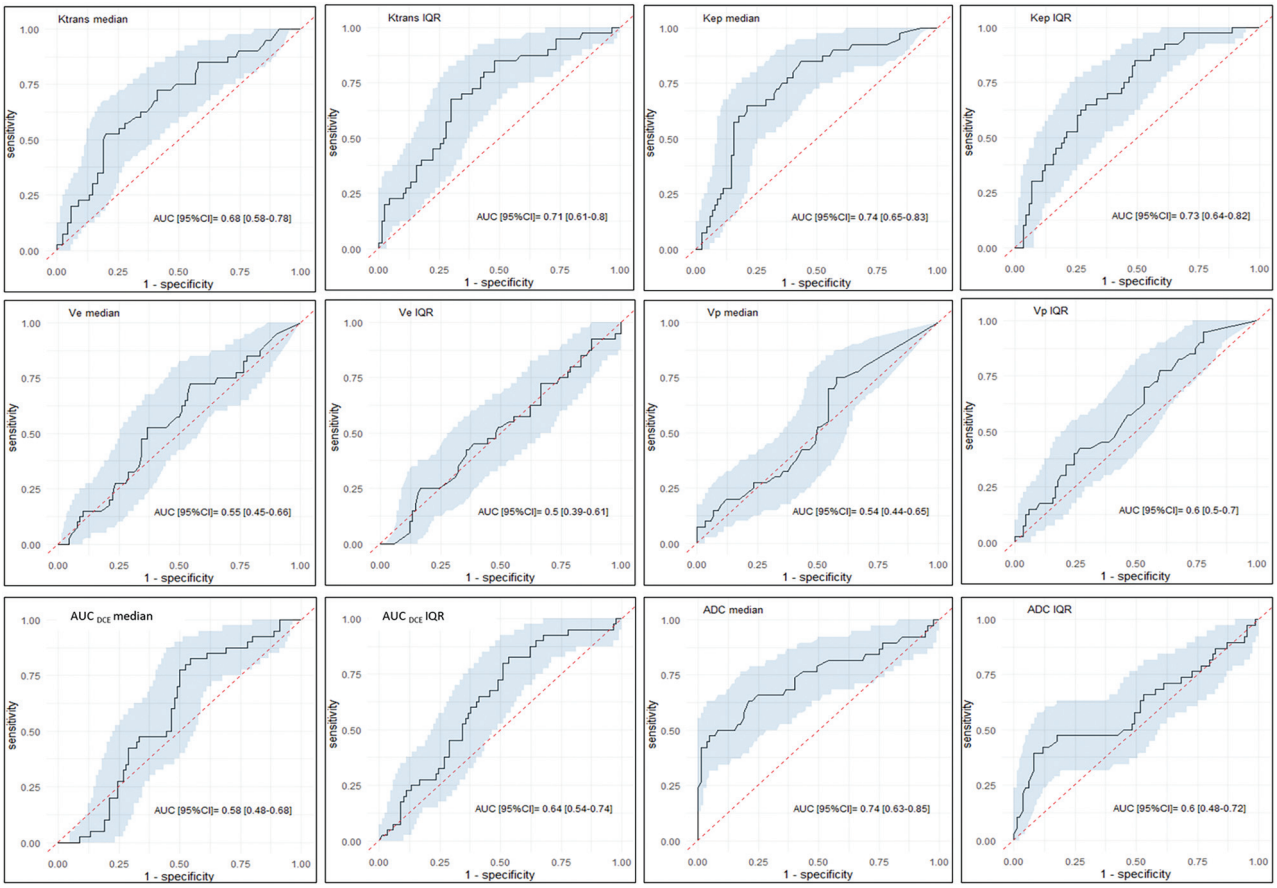

FIG 2. ROC curves of each DCE and ADC parameter when distinguishing malignant from benign lesions. The x-axis refers to 1-specificity, and the y-axis refers to the sensitivity. The *black line* represents the AUC; the *blue area*, the 95% confidence interval; and the *dotted red line*, the diagonal, ie, an AUC of 0.5.

0.25–0.75) with 6 false-negatives. Model G demonstrated a specificity of 0.58 (95% CI, 0.38–0.77) with 11 false-positives.

Interreader Reproducibility. Interreader reproducibility, performed on the distinction between malignant and benign lesions, was good for the IQR of Ve and the median of Vp with an ICC of 0.73 and 0.87, respectively. Interreader reproducibility was excellent for all other quantitative DCE parameters, with an ICC higher than 0.90 (Table 2).

Distinction between Lymphomas and Orbital Inflammations

Univariable Analysis. Among all DCE parameters, the medians of K^{trans} and Kep and the IQR of K^{trans} and Kep were significantly higher in lymphomas compared with orbital inflammations: 1.2 versus 0.6 minute^{-1}, $P = .001$; 2.3 versus 1.1 minute^{-1}, $P < .001$; 1 versus 0.3 minute^{-1}, $P < .001$; and 1.8 versus 0.6 minute^{-1}, $P < .001$, respectively. The detailed data for both groups are given in the Online Supplemental Data.

ROC Curves for Each DCE Parameter. The parameters with the highest AUC were the median of Kep and the IQR of Kep, with AUCs of 0.83 (95% CI, 0.73–0.93) and 0.81 (95% CI, 0.71–0.92), respectively (Online Supplemental Data).

Multivariable Analysis. The training set included 43 patients, and the test set, 20 patients, with 14 and 6 lymphomas, respectively. The model with the highest diagnostic performance was the model D, with an AUC = 0.84 (95% CI, 0.65-0.1), sensitivity = 0.83 (95% CI, 0.5–1), and specificity = 0.85 (95% CI, 0.62–1). The Online Supplemental Data show the diagnostic performance of models evaluated, and the ROC curves are in the Online Supplemental Data.

An example of orbital tumor is provided as Fig 4. Additional examples are also provided in the Online Supplemental Data.

DISCUSSION

Our study showed that DCE is a valuable tool when characterizing orbital lesions, either alone or in combination with morphologic imaging and DWI.

This large prospective work involves the validation process of a new diagnostic imaging tool and biomarkers. Indeed, a few studies already showed the promising results of DCE when characterizing orbital lesions, but most were retrospective, with inherent methodologic bias, and the rare prospective ones included only a small number of patients.[23,30] By confirming the previous results in the literature, our study improves the level of evidence of this technique, facilitating its use in clinical practice. This work suggests that DCE can help distinguish malignant

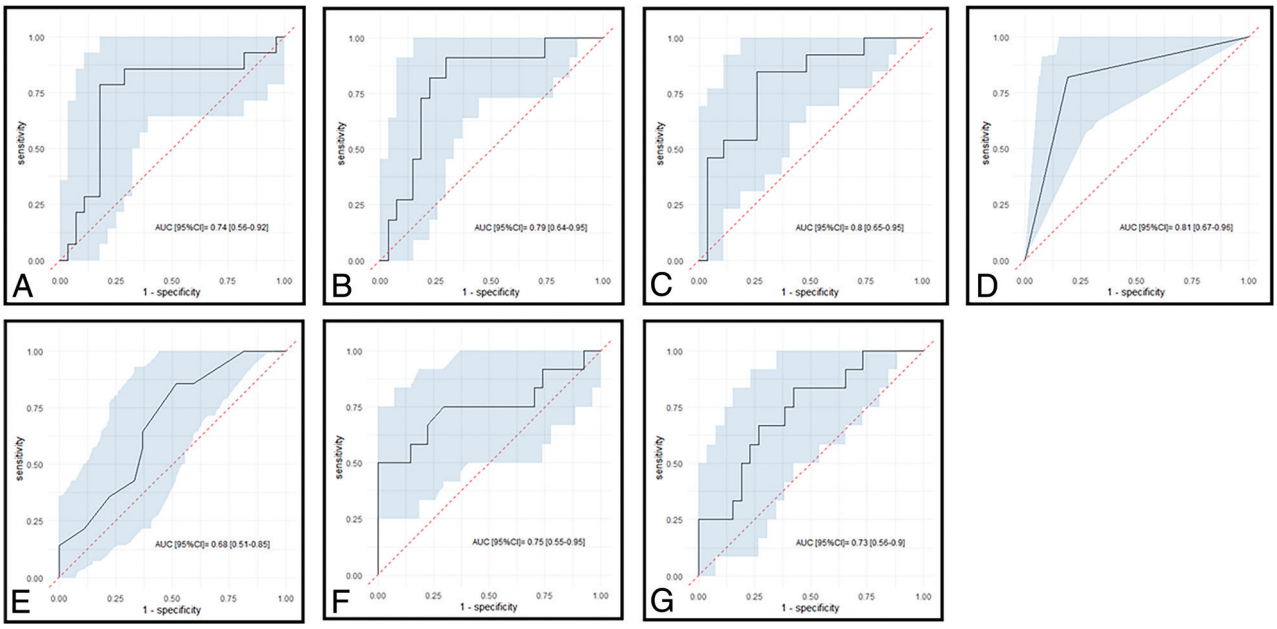

FIG 3. ROC curves of each model when distinguishing malignant from benign lesions. The x-axis refers to 1-specificity; the y-axis, to the sensitivity. The *black line* represents the AUC; the *blue area*, the 95% confidence interval; and the *dotted red line*, the diagonal, ie, an AUC of 0.5. *A* indicates model A with DCE parameters only; *B*, model B with DCE and ADC parameters combined; *C*, model C with DCE and morphologic imaging parameters combined; *D*, model D with DCE, ADC, and morphologic imaging parameters combined; *E*, model E with morphologic imaging parameters only; *F*, model F with ADC only; and *G*, model G with ADC and morphologic imaging parameters.

Table 2: Interobserver reproducibility

K^{trans} (minute^{-1})	
Median (ICC)	0.99
IQR (ICC)	0.96
Kep (minute^{-1})	
Median (ICC)	0.99
IQR (ICC)	0.99
Ve (mL/100 mL of tissue; %)	
Median (ICC)	0.94
IQR (ICC)	0.73
Vp (mL/100 mL of tissue; %)	
Median (ICC)	0.87
IQR (ICC)	0.94
AUC_{DCE} (mmol.min/L)	
Median (ICC)	0.98
IQR (ICC)	0.96
Type of the DCE TIC	
Cohen κ	0.67

from benign lesions, which is in line with findings in previous articles.[19,21,24] Some studies have also suggested that DCE could improve characterization of orbital cavernous venous malformations, schwannomas, or optic pathway gliomas.[15,22,31]

In this study, we decided to distinguish orbital cavernous venous malformation (OCVM) from other venous malformations, defined according the 2018 International Society for the Study of Vascular Anomalies.[32] Indeed, because slow-flow venous malformations of the orbit encompass several distinct diseases including OCVM, the International Society for the Study of Vascular Anomalies classification might be inaccurate in the orbit.[33,34] To avoid any confusion, we used the term OCVM.[35]

Among DCE parameters, Kep was higher in malignant lesions compared with benign ones, in line with previous studies.[19,21,23,25,27] The ROC curve for Kep yielded an AUC of 0.74 versus an AUC of 0.84 reported by Hu et al.[21]

We showed that the constant of transfer from blood plasma to the interstitial environment (K^{trans}) was higher in malignant lesions compared with benign ones and in lymphomas compared with orbital inflammations, also in line with previous studies.[23-25] The ROC curve for K^{trans} yielded an AUC of 0.68, which is a little lower than that of the Kep. Physiopathologically, the K^{trans} reflects both the perfusion and permeability processes. It might be influenced by several vascular factors, making its physiopathologic interpretation challenging. Nevertheless, K^{trans} is one of the most widely used DCE parameters in head and neck diseases for both diagnosis and prognosis.

Most interesting, we showed that the AUC_{DCE} was lower in malignant lesions compared with benign ones and in lymphomas compared with orbital inflammations. The AUC_{DCE} has already shown its usefulness when distinguishing orbital lesions in the literature.[19,23,24] The AUC_{DCE} can be obtained without using any pharmacokinetic models, making it easier to use in clinical practice than the Kep or the K^{trans}. Jittapiromsak et al[19] concluded that the AUC_{DCE} was the best diagnostic criterion and that there was no need for using more complex pharmacokinetic models. However, the ROC curve for the AUC_{DCE} yielded an AUC of 0.58, which is substantially less than that of Kep and K^{trans}. In addition, the AUC_{DCE} is derived from a semiquantitative approach that has limitations, not always having a physical meaning and being mixed measures. The AUC_{DCE} is a combination of the vascular permeability of tissue blood flow and fractional interstitial space.[28] Therefore, we believe that it is probably better to use a pharmacokinetic model. Most postprocessing software is now able to compute DCE data very quickly.

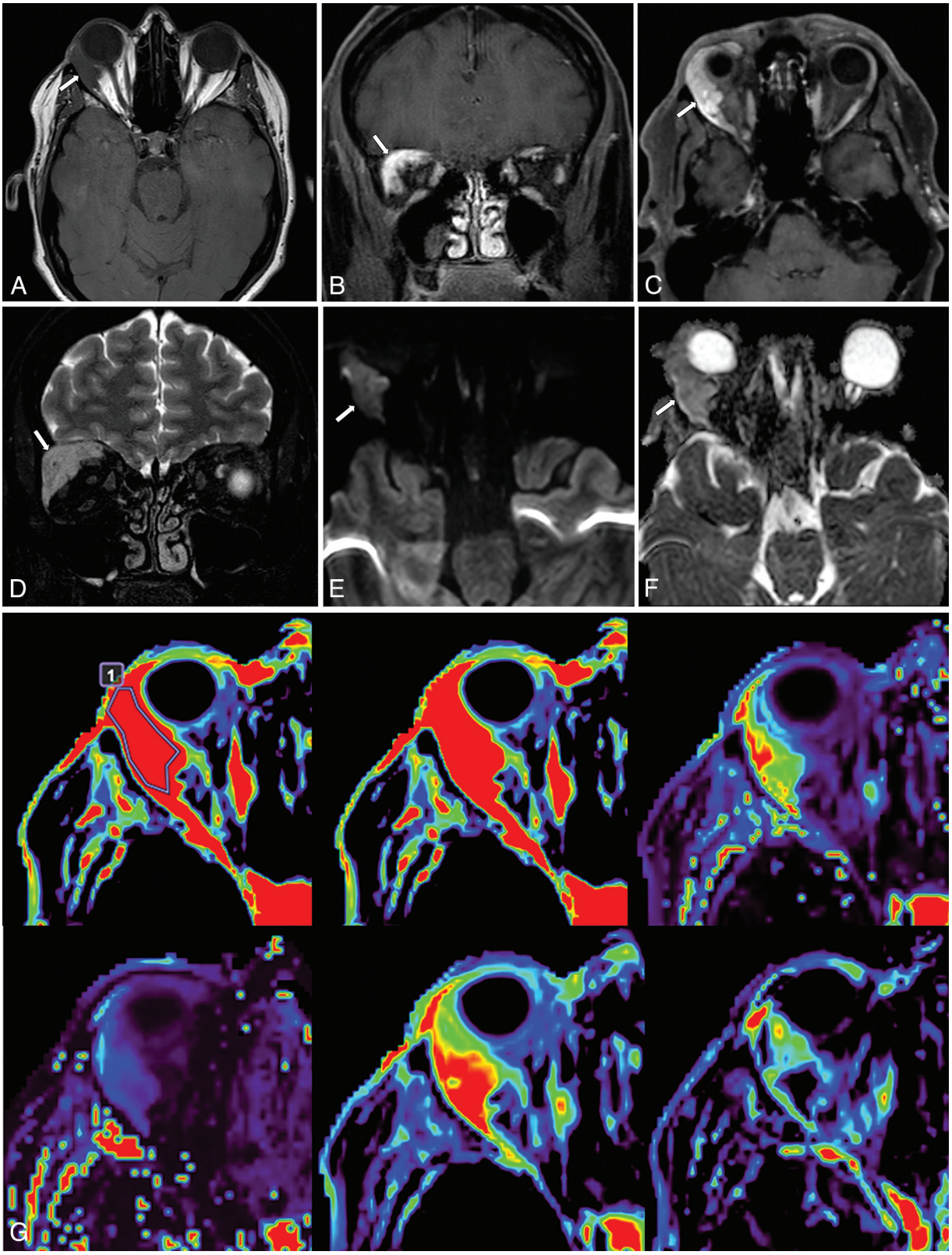

FIG 4. 3T MR imaging in a 45-year-old female patient presenting with vertical diplopia. Axial T1WI (*A*), contrast-enhanced coronal (*B*) and axial (*C*) Dixon T1WI, coronal Dixon T2WI (*D*), axial DWI (*E*), axial ADC (*F*), and DCE MR imaging (*G*) showing a right orbital mass (*arrow*). DCE colorimetric maps are presented as follows from left to right and from top to bottom: AUC_{DCE} with and without the region of interest drawn, K^{trans}, Kep, Ve and Vp. Postsurgery, the final diagnosis was a carcinoma.

In this study the DCE TIC was significantly different in malignant lesions compared with benign ones and in lymphomas compared with orbital inflammations, in line with the literature.[17-19,23]

However, the overlap among the different types of TICs is substantial, making this tool hazardous to use on its own. Indeed, the 3 types of curves are found in each of the groups, not allowing a clinically relevant discrimination. Furthermore, its interobserver reproducibility is limited compared with other DCE parameters, both in this work and in the literature.[36]

Beyond using a single DCE parameter, we showed that a combination of DCE and ADC yielded higher diagnostic performance compared with DCE or ADC alone, which is similar to previous data reported.[16,17,20,23,25] The ADC has proved extremely useful when characterizing orbital lesions, especially for diagnosing orbital lymphomas.[6-9] However, DWI alone failed to correctly classify all malignant lesions such as orbital carcinomas in our study, whereas the combination of DCE and ADC managed to do so. This specific example shows that DCE might translate into a change of management in clinical practice. Moreover, combining DCE and ADC and morphologic imaging features yielded the highest sensitivity among all models when distinguishing malignant from benign lesions and the highest sensitivity and specificity when distinguishing lymphomas from orbital inflammations. Conversely, we showed that models without DCE (morphology alone, ADC alone, or morphology combined with ADC) yielded lower accuracy compared with models with DCE. These results support the importance of performing a comprehensive analysis of all MR imaging data, including a DCE sequence, despite the time cost, when characterizing orbital lesions. This comprehensive approach is in line with 2 radiomics studies showing that all MR imaging sequences provided original and nonredundant features when characterizing orbital lesions and showing that a bag-of-features-based radiomics including DCE data was more effective than without DCE when differentiating ocular adnexal lymphoma and idiopathic orbital inflammation.[26,37]

The duration of our protocol was <20 minutes, which is acceptable. There are no current guidelines regarding the MR imaging protocol when characterizing orbital lesions. On the basis of our study and on the literature data, we suggest that a minimum protocol might include both precontrast and fat-suppressed or Dixon contrast-enhanced T1WI, T2WI, DWI, and DCE imaging, with calculation of the ADC and of at least 1 quantitative parameter such as the Kep or K^{trans}. Postprocessing of both DWI and DCE is now relatively easy and fast, making them usable in clinical practice. It was <1 minute in our study and might be shortened with automatization of the process, which is available on most clinically available postprocessing software. Moreover, this postprocessing might easily be conducted by a technician rather than a radiologist to alleviate the radiologist's workload. We showed that the interobserver reproducibility was high for quantitative DCE parameters and substantially higher than a visual analysis of the type of DCE TIC, in line with the literature.[21] Integrating DCE into clinical practice might help achieve more reliable and reproductible characterization of orbital lesions among various centers worldwide.

Our study has some limitations. First, this is a single-center study including a relatively small number of patients. However, orbital lesions remain rare, thus enrolling patients is challenging. Our study remains a large prospective one evaluating DCE when characterizing orbital lesions. Multicentric prospective studies would be valuable to evaluate the reproducibility of our results. Second, a substantial number of patients initially enrolled in the study and scheduled for surgery did not ultimately undergo surgery after MR imaging but underwent a simple follow-up. Among them, a substantial number of patients had a well-delineated intraconal lesion with typical high signal intensity on T2WI and a progressive centripetal pattern of enhancement easily visible on native DCE MR images, making the diagnosis of orbital cavernous venous malformation almost pathognomonic. Third, the DCE model we used was an extended Tofts model, whereas a study evaluating various DCE models in the orbit showed that the 2CX model was the best-performing one.[24] However, the 2CX model is not available on most postprocessing software, including the Olea Sphere software we used. Fourth, all MR imaging examinations were performed on an optimized 3T MR imaging machine with a 32-channel head coil in a tertiary center specializing in ophthalmology, which might limit the generalization of our results. DCE parameters might vary depending on the type of MR imaging scanner and the type of DCE sequence, so it was not reasonable to provide DCE parameter thresholds for the management of patients with an orbital lesion. Fifth, we performed a DCE sequence with both high spatial and time resolution, which might not be possible on all MR imaging. Further research is needed to evaluate whether a DCE 1.5T MR imaging or one performed with a lower time resolution might achieve equivalent accuracy. Conversely, 7T might help to characterize orbital lesions.[38] Finally, we did not integrate a radiomics analysis into our study, whereas radiomics studies showed high diagnostic performance.[26,39,40]

CONCLUSIONS

This large prospective study confirms that DCE MR imaging is a valuable tool when characterizing orbital lesions. It can be a complementary source of information and can improve the diagnostic capabilities of 3T MR imaging when characterizing orbital lesions, in particular in combination with DWI. DCE should be considered in clinical practice to improve the diagnosis of orbital lesions. This work participates in the validation process of a new diagnostic imaging tool and biomarkers. It contributes to improving the level of evidence of this technique, and it might help accelerate the adoption of DCE in imaging protocols in all centers worldwide when characterizing orbital lesions.

ACKNOWLEDGMENTS

We acknowledge Souhila Silem and Bahia Abdat, clinical research technicians in the Department of Clinical Research, Rothschild Foundation Hospital, Paris, France, for actively contributing to this study.

Disclosure forms provided by the authors are available with the full text and PDF of this article at www.ajnr.org.

REFERENCES

1. Shields JA, Shields CL, Scartozzi R. **Survey of 1264 patients with orbital tumors and simulating lesions.** *Ophthalmology* 2004;111:997–1008 CrossRef Medline
2. Demirci H, Shields CL, Shields JA, et al. **Orbital tumors in the older adult population.** *Ophthalmology* 2002;109:243–48 CrossRef Medline
3. Kansakar P, Sundar G. **Vision loss associated with orbital surgery: a major review.** *Orbit* 2020;39:197–208 CrossRef Medline
4. Purgason PA, Hornblass A. **Complications of surgery for orbital tumors.** *Ophthalmic Plast Reconstr Surg* 1992;8:88–93 CrossRef Medline
5. Lecler A, Boucenna M, Lafitte F, et al. **Usefulness of colour Doppler flow imaging in the management of lacrimal gland lesions.** *Eur Radiol* 2017;27:779–89 CrossRef Medline
6. Jaju A, Rychlik K, Ryan ME. **MRI of pediatric orbital masses: role of quantitative diffusion-weighted imaging in differentiating benign from malignant lesions.** *Clin Neuroradiol* 2020;30:615–24 CrossRef Medline
7. Eissa L, Abdel Razek AA, Helmy E. **Arterial spin labeling and diffusion-weighted MR imaging: utility in differentiating idiopathic orbital inflammatory pseudotumor from orbital lymphoma.** *Clin Imaging* 2021;71:63–68 CrossRef Medline
8. ElKhamary SM, Galindo-Ferreiro A, AlGhafri L, et al. **Characterization of diffuse orbital mass using apparent diffusion coefficient in 3-Tesla MRI.** *Eur J Radiol Open* 2018;5:52–57 CrossRef Medline
9. Phuttharak W, Boonrod A, Patjanasoontorn N, et al. **The roles of the diffusion-weighted imaging in orbital masses.** *J Med Imaging Radiat Oncol* 2017;61:753–58 CrossRef Medline
10. Lecler A, Duron L, Zmuda M, et al. **Intravoxel incoherent motion (IVIM) 3T MRI for orbital lesion characterization.** *Eur Radiol* 2021;31:14–23 CrossRef Medline
11. Soussan JB, Deschamps R, Sadik JC, et al. **Infraorbital nerve involvement on magnetic resonance imaging in European patients with IgG4-related ophthalmic disease: a specific sign.** *Eur Radiol* 2017;27:1335–43 CrossRef Medline
12. Sepahdari AR, Aakalu VK, Setabutr P, et al. **Indeterminate orbital masses: restricted diffusion at MR imaging with echo-planar diffusion-weighted imaging predicts malignancy.** *Radiology* 2010;256:554–64 CrossRef Medline
13. Shor N, Sené T, Zuber K, et al. **Discriminating between IgG4-related orbital disease and other causes of orbital inflammation with intra voxel incoherent motion (IVIM) MR imaging at 3T**. *Diagn Interv Imaging* 2021;102:727–34 CrossRef Medline
14. Cuenod CA, Balvay D. **Perfusion and vascular permeability: basic concepts and measurement in DCE-CT and DCE-MRI.** *Diagn Interv Imaging* 2013;94:1187–204 CrossRef Medline
15. Jost SC, Ackerman JW, Garbow JR, et al. **Diffusion-weighted and dynamic contrast-enhanced imaging as markers of clinical behavior in children with optic pathway glioma.** *Pediatr Radiol* 2008;38:1293–99 CrossRef Medline
16. Xu XQ, Hu H, Liu H, et al. **Benign and malignant orbital lymphoproliferative disorders: differentiating using multiparametric MRI at 3.0T.** *J Magn Reson Imaging* 2016;45:167–76 CrossRef Medline
17. Li X, Wu X, Qian J, et al. **Differentiation of lacrimal gland tumors using the multi-model MRI: classification and regression tree (CART)-based analysis.** *Acta Radiol* 2022;63:923–32 CrossRef Medline
18. Yuan Y, Kuai XP, Chen XS, et al. **Assessment of dynamic contrast-enhanced magnetic resonance imaging in the differentiation of malignant from benign orbital masses.** *Eur J Radiol* 2013;82:1506–11 CrossRef Medline
19. Jittapiromsak N, Hou P, Liu HL, et al. **Dynamic contrast-enhanced MRI of orbital and anterior visual pathway lesions.** *Magn Reson Imaging* 2018;51:44–50 CrossRef Medline
20. Haradome K, Haradome H, Usui Y, et al. **Orbital lymphoproliferative disorders (OLPDs): value of MR imaging for differentiating orbital lymphoma from benign OPLDs.** *AJNR Am J Neuroradiol* 2014;35:1976–82 CrossRef Medline
21. Hu H, Xu XQ, Liu H, et al. **Orbital benign and malignant lymphoproliferative disorders: differentiation using semi-quantitative and quantitative analysis of dynamic contrast-enhanced magnetic resonance imaging.** *Eur J Radiol* 2017;88:88–94 CrossRef Medline
22. Xian J, Zhang Z, Wang Z, et al. **Evaluation of MR imaging findings differentiating cavernous haemangiomas from schwannomas in the orbit.** *Eur Radiol* 2010;20:2221–28 CrossRef Medline
23. Ro SR, Asbach P, Siebert E, et al. **Characterization of orbital masses by multiparametric MRI.** *Eur J Radiol* 2016;85:324–36 CrossRef Medline
24. Lecler A, Balvay D, Cuenod CA, et al. **Quality-based pharmacokinetic model selection on DCE-MRI for characterizing orbital lesions.** *J Magn Reson Imaging* 2019;50:1514–25 CrossRef Medline
25. Wang Y, Song L, Guo J, et al. **Value of quantitative multiparametric MRI in differentiating pleomorphic adenomas from malignant epithelial tumors in lacrimal gland.** *Neuroradiology* 2020;62:1141–47 CrossRef Medline
26. Hou Y, Xie X, Chen J, et al. **Bag-of-features-based radiomics for differentiation of ocular adnexal lymphoma and idiopathic orbital inflammation from contrast-enhanced MRI.** *Eur Radiol* 2021;31:24–33 CrossRef Medline
27. Qian W, Xu XQ, Hu H, et al. **Dynamic contrast-enhanced MRI in orbital lymphoproliferative disorders: effects of region of interest selection methods on time efficiency, measurement reproducibility, and diagnostic ability.** *J Magn Reson Imaging* 2018;47:1298–305 CrossRef Medline
28. Gaddikeri S, Gaddikeri RS, Tailor T, et al. **Dynamic contrast-enhanced MR imaging in head and neck cancer: techniques and clinical applications.** *AJNR Am J Neuroradiol* 2016;37:588–95 CrossRef Medline
29. Benchoufi M, Matzner-Lober E, Molinari N, et al. **Interobserver agreement issues in radiology.** *Diagn Interv Imaging* 2020;101:639–41 CrossRef Medline
30. Russo C, Strianese D, Perrotta M, et al. **Multi-parametric magnetic resonance imaging characterization of orbital lesions: a triple blind study.** *Semin Ophthalmol* 2020;35:95–102 CrossRef Medline
31. Tanaka A, Mihara F, Yoshiura T, et al. **Differentiation of cavernous hemangioma from schwannoma of the orbit: a dynamic MRI study.** *AJR Am J Roentgenol* 2004;183:1799–804 CrossRef Medline
32. International Society for the Study of Vascular Anomalies. **Classification.** https://www.issva.org/classification. Accessed August 26, 2023
33. Tawfik HA, Dutton JJ. **Orbital vascular anomalies: a nomenclatorial, etiological, and nosologic conundrum.** *Ophthalmic Plast Reconstr Surg* 2022;38:108–21 CrossRef Medline
34. Steele L, Zbeidy S, Thomson J, et al. **How is the term haemangioma used in the literature? An evaluation against the revised ISSVA classification.** *Pediatr Dermatol* 2019;36:628–33 CrossRef Medline
35. Elbaze S, Duron L, Mambour N, et al. **A signature of structural MRI features at 3 Tesla allows an accurate characterization of orbital cavernous venous malformation.** *Eur Radiol* 2023;33:2149–59 CrossRef Medline
36. Xian J, Zhang Z, Wang Z, et al. **Value of MR imaging in the differentiation of benign and malignant orbital tumors in adults.** *Eur Radiol* 2010;20:1692–702 CrossRef Medline
37. Lecler A, Duron L, Balvay D, et al. **Combining multiple magnetic resonance imaging sequences provides independent reproducible radiomics features.** *Sci Rep* 2019;9:2068 CrossRef Medline
38. Lecler A, Duron L, Charlson E, et al. **Comparison between 7 Tesla and 3 Tesla MRI for characterizing orbital lesions.** *Diagn Interv Imaging* 2022;103:433–39 CrossRef Medline
39. Duron L, Heraud A, Charbonneau F, et al. **A magnetic resonance imaging radiomics signature to distinguish benign from malignant orbital lesions.** *Invest Radiol* 2021;56:173–80 CrossRef Medline
40. Duron L, Savatovsky J, Fournier L, et al. **Can we use radiomics in ultrasound imaging? Impact of preprocessing on feature repeatability.** *Diagn Interv Imaging* 2021;102:659–67 CrossRef Medline